

Predictive multi-hazard hurricane data-based fragility model for residential homes

Carol C. Massarra^a, Carol J. Friedland^{a,*}, Brian D. Marx^b, J. Casey Dietrich^c

^a Bert S. Turner Department of Construction Management, Louisiana State University, Baton Rouge, LA, 70803, USA

^b Department of Experimental Statistics, Louisiana State University, Baton Rouge, LA, 70803, USA

^c Department of Civil, Construction, and Environmental Engineering, North Carolina State University, Raleigh, NC, 27695, USA

ARTICLE INFO

Keywords:

Predictive fragility models
Data-based statistical models
Residential buildings
Hurricane hazards

ABSTRACT

Multi-hazard hurricane data-based fragility models are able to represent multiple predictor variables, be validated based on observed data, and consider variability in building characteristics and hazard variables. This paper develops predictive hurricane, multi-hazard, single-family building fragility models for ordered categorical damage states (DS) and binary complete failure/non-complete failure using proportional odds cumulative logit and logistic regression models, respectively. In addition to their simplicity, these models are able to represent multiple hurricane hazard variables and include variable interactions, thus improving model fitting and damage prediction. Surveys of physical damage in coastal Mississippi following Hurricane Katrina (2005) and high-resolution numerical hindcast hazard intensities from the Simulating WAVes Nearshore and Advanced CIRCulation (SWAN + ADCIRC) models are used as model input. Prediction accuracy is expressed in terms of cross-validation (CV) and evaluated using leave-one-out cross-validation (LOOCV).

Thirty-nine combinations of global damage response variables were investigated. Of these models, six DS and one complete failure model met the evaluation criteria. Maximum significant wave height was the only significant hazard variable for the DS models, while maximum 3-s gust wind speed, maximum surge depth, and maximum water speed were found to be significant predictors for the complete failure model. Model prediction external accuracy ranged from 81% to 87%.

1. Introduction

Fragility models are used to estimate the probability of collapse or being in or exceeding a specified damage state, conditional upon one or more hazards. The models are developed either from statistical analysis of observed field data (i.e., data-based models) or through mechanics-based analysis and stochastic simulation techniques (i.e., analytical models). Vulnerability and fragility models have been most often developed for wind (e.g., Crandell, 1998; Khanduri and Morrow, 2003; Lee and Rosowsky, 2005; van de Lindt and Dao, 2009; Pita et al., 2011; Masoomi and van de Lindt, 2016; Masoomi et al., 2018; Memari et al., 2018) or flood (e.g., van de Lindt and Taggart, 2009; Pistrika and Jonkman, 2010; Merz et al., 2013) separately, rather than for the combined effects of wind, surge, and waves. The damage generated by multi-hazard events may be greater than the aggregation of damage caused by each hazard separately (Kappes et al., 2012a, 2012b); therefore, multi-hazard vulnerability and fragility models are needed.

However, in current literature, building vulnerability or fragility has been primarily considered from an analytical perspective (e.g., Lee and Rosowsky, 2006; Li and Ellingwood, 2009b, 2009a; Li et al., 2011; Schmidt et al., 2011; Li and van de Lindt, 2012; Barbato et al., 2013; Choine et al., 2015; Liu et al., 2015). These models are developed by modeling an individual building or an array of buildings through parametric modeling, where building response as a result of increasing hazard load is documented in the form of fragility functions. These functions are highly dependent upon structural and hazard characteristics, as well as the probabilistic parameters selected to represent uncertainty. However, significant modeling challenges remain, including derivation of the joint hazard distribution, consideration of overlapping spatial and temporal hazard effects, validation of developed models, and reflection of the population and variability of the built environment, requiring significant input data and computation capabilities. These issues hinder the development of comprehensive multi-hazard hurricane fragility models.

* Corresponding author. Bert S. Turner Department of Construction Management, Louisiana State University, 3316-B Patrick F. Taylor Hall, Baton Rouge, LA, 70803, USA.

E-mail addresses: cmassa1@lsu.edu (C.C. Massarra), friedland@lsu.edu (C.J. Friedland), bmarx@lsu.edu (B.D. Marx), jcdietrich@ncsu.edu (J.C. Dietrich).

<https://doi.org/10.1016/j.coastaleng.2019.04.008>

Received 26 October 2017; Received in revised form 18 April 2019; Accepted 22 April 2019

Available online 06 May 2019

0378-3839/© 2019 Published by Elsevier B.V.

Fragility models have been considered infrequently from a statistical perspective, although current efforts support the validation of analytical models and development of robust statistical models. Examples of these efforts to collect and catalog hazard and building damage data include the Natural Hazards Engineering Research Infrastructure (NHERI) DesignSafe, National Institute of Standards and Technology (NIST) Disaster and Failure Studies Data Repository (NIST, 2011), and the Pacific Earthquake Engineering Research (PEER) Center Ground Motion Database (PEER, 2011). Data-based statistical models represent damage as a function of multiple hazards, use observed data to fit the model and assess its prediction accuracy, and consider variability in building and environmental attributes (Pitilakis et al., 2014). These characteristics are of particular value for non-engineered or marginally engineered buildings (e.g., houses), where building parameters are unavailable or impractical to model for individual buildings. Data-based models have been widely used to model building damage from tsunami (e.g., Reese et al., 2007; Koshimura et al., 2009; Reese et al., 2011; Suppasri et al., 2012; Suppasri et al., 2013; Charvet et al., 2014a; Charvet et al., 2014b; Charvet et al., 2015; Muhari et al., 2015) and earthquake (Porter et al., 2007; Tang et al., 2012; Lallemand et al., 2015) hazards, and less frequently for hurricane hazards (e.g., Tomiczek et al., 2014b; Hatzikyriakou et al., 2015; Tomiczek et al., 2017; Hatzikyriakou and Lin, 2018). Although not specific to buildings, data-based models have been used to model fragility of power systems (Reed et al., 2016) and oil storage tanks (Kameshwar and Padgett, 2018) for hurricane hazards.

In current literature, hurricane data-based fragility models are classified as explanatory or predictive models. Explanatory models are developed primarily for inference and interpretation of model coefficients in the same population from which sample data are obtained, where model performance is validated on the same set of buildings used to develop the model. On the other hand, predictive models are developed for use in populations outside that used to obtain sample data. The model's performance is externally validated on a new sample of buildings. Said differently, the training model is applied to test data for external predictive or classification purposes. Unlike explanatory models, predictive models are opportunistically built with the goal of predicting future damage for a new set of buildings in a hazard environment. Assessment of predictive models is measured by the predictive accuracy, often using metrics computed from external cross-validation (Stone, 1974; Geisser, 1975).

Within existing data-based fragility models, dependent variables are treated either as multinomial categorical ordered damage states (e.g., Tomiczek et al., 2017; Hatzikyriakou and Lin, 2018) or as binomial collapse/non-collapse (e.g., Tomiczek et al., 2014a; Hatzikyriakou et al., 2015; Reed et al., 2016), while the explanatory variables are combinations of hazard parameters and environmental and building attributes. Existing models primarily focus on inference and interpretation of model coefficients without evaluation of model performance. While inference and interpretation provide insight on the effect of explanatory variables on damage, external validation is needed to evaluate model performance, thus providing a realistic evaluation of model prediction accuracy for future events. Additionally, categorical dependent variables have been modeled as continuous numerical variables (e.g., Tomiczek et al., 2014a; Tomiczek et al., 2017) _ENREF_71, which may result in probabilities greater than one or less than zero, and can have inefficient standard errors for the estimated coefficients because the discrete nature of the response is not modeled.

Specific to residential buildings subjected to surge and wave hazards, Tomiczek et al. (2014a) fitted and compared six multiple linear regression models to estimate the probability of collapse for pile-elevated, wood-framed buildings as a function of combinations of maximum significant wave height, breaking wave height, maximum current velocity, freeboard height, and building age. Freeboard height above wave crests, maximum significant wave height, maximum current velocity, and construction date were found to be the most important

variables that contribute significantly to probability of collapse. Tomiczek et al. (2017) classified building damage into seven DS and used multiple linear regression to estimate probability of damage as a function of relative shielding, age, maximum water velocity, maximum water depth, and minimum freeboard. Maximum water velocity and relative shielding were found to be the most important variables that significantly contribute to building damage.

However, in both previous studies, the categorical dependent variables (non-collapse/collapse and the seven DS) were modeled as continuous numerical variables. Additionally, a measurement of relative residual variance to evaluate model fitting was used. While relative residual variance can be useful for comparison across models, it may be of limited use for prediction accuracy due to the discrete nature of the response variable.

Specific to residential buildings subjected to wind, surge, wave, and rain hazards, Hatzikyriakou et al. (2015) developed a component-based logistic regression fragility model to predict the probability of collapse for single-family home foundations, exterior walls, and siding as a function of environmental and building attributes, namely, distance from the coast, ground elevation, elevation of the lowest horizontal member, structure height above lowest horizontal member, house age, and building perimeter. Distance from the coast, ground elevation, and house age were found to be significant damage predictors for component failure. Although the categorical binary response variable was modeled correctly, the model was limited to inference and interpretation of the model coefficients without any evaluation of model performance. Additionally, hurricane hazard parameters were not evaluated.

A general deficiency within current hurricane data-based fragility models is twofold: (1) The crude use of classical modeling approaches for what is truly a binomial or multinomial response, and (2) the limited evaluation of model performance using external validation. Specifically, while multiple linear regression explains the relationship between damage and explanatory variables, logistic regression and proportional odds cumulative logit models represent the true nature and distribution of the response variable, while also providing meaningful interpretations in terms of odds ratios. While model fit is paramount, external validity provides a realistic evaluation of model prediction accuracy when applied to field data, for example to predict future damage. In this context, external validation is an improvement over the current multi-hazard data-based fragility models.

In this research, predictive multi-hazard, hurricane-data-based, fragility models for single-family homes are developed for ordered categorical damage states (DS) and binary complete failure/non-complete failure. The models are developed as a function of maximum hurricane hazard variables (i.e., wind speed, significant wave height, surge depth, water speed) at the individual building scale. Single family home damage states assessed from recorded videographic data and NOAA aerial imagery collected in coastal Mississippi after Hurricane Katrina (2005), along with simulated hazard data computed by the tightly-coupled Simulating WAVes Nearshore and ADvanced CIRCulation (SWAN + ADCIRC) model are used as model inputs. Data collection using a videographic approach has been previously used in multiple post-disaster studies (e.g., Curtis et al., 2007a; Curtis et al., 2007b; Curtis et al., 2010) and aerial imagery has been shown to be effective for assessing roof damage (Womble et al., 2006). SWAN + ADCIRC joint models have been used to simulate hazards intensities for the development of fragility models (Tomiczek et al., 2014a, 2017; Hatzikyriakou and Lin, 2018; Masoomi et al., 2018). Global building damage (i.e., description of the overall building damage) is assessed using the seven-category Wind and Flood (WF) Damage Scale developed by Friedland and Levitan (2009). The probability of being in or exceeding a specified DS and the probability of complete failure are estimated using proportional odds cumulative logit and logistic regression models, respectively. External cross-validation (CV) is performed to evaluate model prediction accuracy, specifically using “leave-one-out” cross-validation (LOOCV) and expressed in terms of the cross-

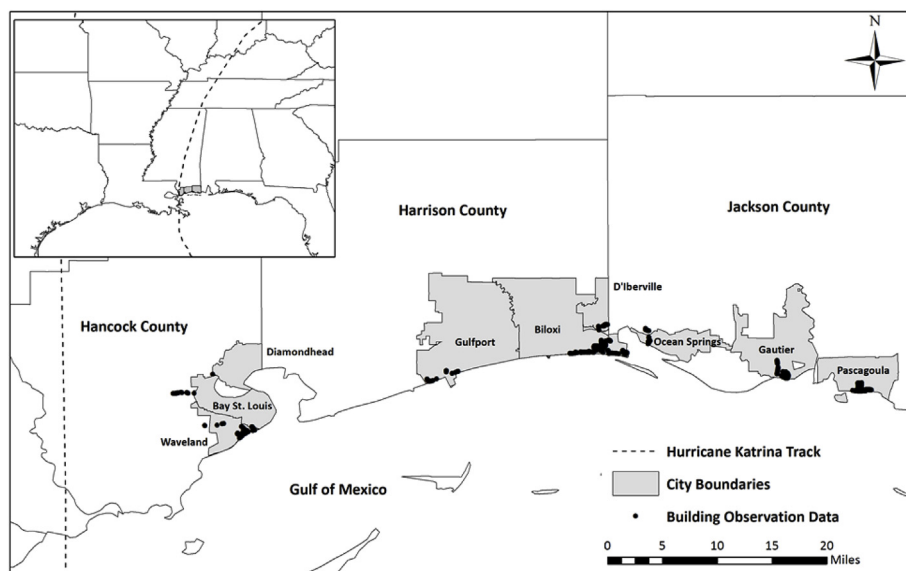


Fig. 1. Hurricane Katrina track, study areas, and building observation locations.

classification rate (CCR).

2. Data

2.1. Global building damage state response variable

Hurricane Katrina made landfall on 29 August 2005 as a Saffir-Simpson Category 3 hurricane with 1-min sustained winds of 56 m/s (124 mph) near Buras, Louisiana, and then as a Category 3 hurricane with 53 m/s (118 mph) 1-min sustained winds near the Louisiana-Mississippi border with storm surge depth of 8.5 m (28 feet) at Pass Christian, Mississippi (Fritz et al., 2008). An MCEER rapid reconnaissance was conducted on 6–11 September 2005 using the VIEWS™ system (Adams et al., 2004) to capture georeferenced video of buildings in coastal Mississippi, specifically Hancock, Harrison, and Jackson Counties (Fig. 1).

The field data collection consisted of acquisition of geo-referenced high-resolution video captured from the passenger side of a slowly moving vehicle. The goal of the reconnaissance was to document the extent of damage in the near aftermath of the hurricane. No specific sampling strategy was implemented and the collected data reflect limitations of accessibility and data collection time, including impassibility of routes and the presence of debris piles and emergency vehicles obscuring data collection. Therefore, a degree of uncertainty is inherent in the data collection and damage assessment that is considered in the overall sampling error but not explicitly evaluated in this analysis.

The building damage assessment was based on rapid damage assessment rather than detailed damage assessment. Rapid building damage assessment relies on an exterior evaluation of the structure unless the structure's condition cannot be adequately viewed from the

exterior. The overall observed conditions are used to evaluate the building's general condition (e.g., totally collapsed, partially collapsed, minor, moderate). Every building along the driving route was surveyed by assessing damage to the portions of the buildings captured on the videos (e.g., front and side of the building). Building roof damage was assessed using post-event National Oceanic and Atmospheric Administration (NOAA) aerial color images with 0.3 m spatial resolution. The global building DS response variable (Y) was derived from visual damage assessment of each surveyed building using the Wind and Flood (WF) Damage Scale developed by Friedland and Levitan (2009). The WF Damage Scale divides damage state data into three categories: physical damage state, stillwater (i.e., flood only) damage state, and final combined damage state. The physical damage state describes the observable damage resulting from wind or flood (including high velocity and wave action) to the following components: roof cover, windows and doors, roof deck, foundation, appurtenant structures, wall cladding, wall structure, roof structure, and overall structural damage. The damage states that describe this physical damage range from WF-0 to WF-6. The stillwater damage state depends only on the depth of flooding for slow rising floodwaters without velocity or wave action to cause physical damage. The damage states that describe stillwater flood damage range from WF-2 to WF-6 the shaded cells the WF Damage Scale are used for classification only, whereas non-shaded cells provide typical values. The final combined damage state is the maximum between the physical damage state and the stillwater damage state. The WF Damage Scale has also been further modified and applied by Tomiczek et al. (2017) Zhang et al. (2017), and Hatzikyriakou (2017) to classify building damage data obtained from field reconnaissance. Buildings in the study area were assessed by two assessors to assess inter-evaluator error. A confusion matrix that shows the percentage of classification error (CE) for each damage state

Table 1

Assessor 1 vs. Assessor 2 error matrices, class error (CE), and cross classification rate.

Assessor 2	Assessor 1								Sum	CE	CCR
	WF0	WF1	WF2	WF3	WF4	WF5	WF6				
WF0	4	0	0	0	0	0	0	4	0%		
WF1	0	7	0	0	0	0	0	7	0%		
WF2	0	0	58	1	1	0	0	60	3%		
WF3	0	0	0	347	1	1	0	349	1%		
WF4	0	0	0	2	43	0	0	45	4%		
WF5	0	0	0	0	1	41	0	42	2%		
WF6	0	0	0	0	0	0	359	359	0%	99%	

Table 2

Frequency and percentages of observed (η) or missingness (λ) for foundation, number of stories, and cladding type found in Hancock, Harrison, and Jackson counties.

County	Hancock	Harrison	Jackson	Total
	Frequency (η or λ)	Frequency (η or λ)	Frequency (η or λ)	
Slab	39 (21%)	86 (23%)	151 (50%)	276
Elevated Floor	56 (30%)	130 (34%)	40 (13%)	266
Missing	89 (48%)	163 (43%)	112 (37%)	364
One-Story	26 (14%)	160 (42%)	187 (62%)	373
Two-Story	15 (8%)	39 (10%)	45 (15%)	99
Missing	143 (78%)	180 (47%)	71 (23%)	394
Siding	47 (26%)	176 (46%)	136 (45%)	359
Brick	2 (1%)	40 (11%)	99 (33%)	141
Missing	135 (73%)	163 (43%)	68 (22%)	366

and the cross classification rate (CCR, %) between the two assessors is presented in Table 1. The results show that the overall CCR between the two assessors is high (99%) with highest CE for damage state WF4 (4%).

The study area was limited to the initial surge inundation extents delineated by the Federal Emergency Management Agency (FEMA). A geographic information systems (GIS) database was developed that includes land parcel data and building footprint polygons. The calculated centroid for each building footprint was used to represent the building location in the study area. Single-family homes were typically wood-framed, one-and two-story homes with brick or siding cladding, and built on slabs or elevated foundations. Missing foundation type and number of stories were found in the study area. Table 2 gives a detailed description of the frequency and percentage of observed (η) or missingness (λ) for foundation, number of stories, and cladding type in each county of the study area.

Few buildings with foundation types and numbers of stories differing from these predominant characteristics were found in the study area. Such buildings, along with those having unassessed DS, were excluded from the analysis, resulting in a final dataset describing the global building DS for 866 single-family homes (Table 3).

For categorical variables, it is generally recommended that a minimum of 50 samples be collected for each variable level (Lillesand et al., 2014). However, low sample numbers in WF0, WF1, WF4, and WF5 indicate that issues in model fitting may be encountered. Therefore, WF DS were aggregated to represent the global building DS response variable Y for n models, each with j levels, $DS_{j,n}$ (Table 4). Models 1 through 37 have ordered multinomial response variables, while Models 38 and 39 have a binary response variable.

2.2. Computationally modeled explanatory hazard variables

Hazard attributes were characterized via a coupled modeling system for hurricane winds, waves, and storm surge (Bunya et al., 2010; Dietrich et al., 2010). This system represents the coastal environment with varying levels of resolution to predict the storm-induced development of waves and surge in open water and then their interactions

Table 3

Global building damage states and frequency of collected data.

Levels, j	Damage states with percentage of buildings in each level	Number of Buildings	Percent of Buildings
1	WF0=No damage	4	0.46%
2	WF1 = Minor damage	7	0.81%
3	WF2=Moderate damage	60	6.96%
4	WF3=Severe damage	349	40.30%
5	WF4=Very severe damage	45	5.20%
6	WF5=Partial collapse	42	4.85%
7	WF6= Collapse	359	41.45%

Table 4

Model (n), number of observations in each WF DS, and global building DS response variable levels for each model, $DS_{j,n}$.

Model (n)	WF0	WF1	WF2	WF3	WF4	WF5	WF6
No. Obs.	4	7	60	349	45	42	359
1	$DS_{1,1}$	$DS_{2,1}$	$DS_{3,1}$	$DS_{4,1}$	$DS_{5,1}$	$DS_{6,1}$	$DS_{7,1}$
2	$DS_{1,2}$			$DS_{2,2}$	$DS_{3,2}$	$DS_{4,2}$	$DS_{5,2}$
3	$DS_{1,3}$			$DS_{2,3}$	$DS_{3,3}$	$DS_{4,3}$	
4	$DS_{1,4}$			$DS_{2,4}$		$DS_{3,4}$	
5	$DS_{1,5}$			$DS_{2,5}$		$DS_{3,5}$	$DS_{4,5}$
6	$DS_{1,6}$			$DS_{2,6}$	$DS_{3,6}$		
7	$DS_{1,7}$			$DS_{2,7}$			$DS_{3,7}$
8	$DS_{1,8}$				$DS_{2,8}$	$DS_{3,8}$	$DS_{4,8}$
9	$DS_{1,9}$				$DS_{2,9}$		$DS_{3,9}$
10	$DS_{1,10}$				$DS_{2,10}$	$DS_{3,10}$	
11	$DS_{1,11}$		$DS_{2,11}$	$DS_{3,11}$	$DS_{4,11}$	$DS_{5,11}$	$DS_{6,11}$
12	$DS_{1,12}$		$DS_{2,12}$		$DS_{3,12}$	$DS_{4,12}$	$DS_{5,12}$
13	$DS_{1,13}$		$DS_{2,13}$			$DS_{3,13}$	$DS_{4,13}$
14	$DS_{1,14}$		$DS_{2,14}$				$DS_{3,14}$
15	$DS_{1,15}$		$DS_{2,15}$		$DS_{3,15}$		$DS_{4,15}$
16	$DS_{1,16}$		$DS_{2,16}$			$DS_{3,16}$	
17	$DS_{1,17}$		$DS_{2,17}$		$DS_{3,17}$		
18	$DS_{1,18}$		$DS_{2,18}$	$DS_{3,18}$		$DS_{4,18}$	
19	$DS_{1,19}$		$DS_{2,19}$	$DS_{3,19}$			$DS_{4,19}$
20	$DS_{1,20}$		$DS_{2,20}$	$DS_{3,20}$	$DS_{4,20}$		
21	$DS_{1,21}$		$DS_{2,21}$	$DS_{3,21}$	$DS_{4,21}$		$DS_{5,21}$
22	$DS_{1,22}$		$DS_{2,22}$	$DS_{3,22}$		$DS_{4,22}$	$DS_{5,22}$
23	$DS_{1,23}$		$DS_{2,23}$	$DS_{3,23}$	$DS_{4,23}$	$DS_{5,23}$	
24	$DS_{1,24}$	$DS_{2,24}$		$DS_{3,24}$	$DS_{4,24}$	$DS_{5,24}$	$DS_{6,24}$
25	$DS_{1,25}$	$DS_{2,25}$			$DS_{3,25}$	$DS_{4,25}$	$DS_{5,25}$
26	$DS_{1,26}$	$DS_{2,26}$				$DS_{3,26}$	$DS_{4,26}$
27	$DS_{1,27}$	$DS_{2,27}$					$DS_{3,27}$
28	$DS_{1,28}$	$DS_{2,28}$		$DS_{3,28}$		$DS_{4,28}$	
29	$DS_{1,29}$	$DS_{2,29}$		$DS_{3,29}$			$DS_{4,29}$
30	$DS_{1,30}$	$DS_{2,30}$		$DS_{3,30}$			
31	$DS_{1,31}$	$DS_{2,31}$		$DS_{3,31}$	$DS_{4,31}$		$DS_{5,31}$
32	$DS_{1,32}$	$DS_{2,32}$		$DS_{3,32}$	$DS_{4,32}$		
33	$DS_{1,33}$	$DS_{2,33}$		$DS_{3,33}$	$DS_{4,33}$	$DS_{5,33}$	
34	$DS_{1,34}$	$DS_{2,34}$	$DS_{3,34}$		$DS_{4,34}$	$DS_{5,34}$	$DS_{6,34}$
35	$DS_{1,35}$	$DS_{2,35}$	$DS_{3,35}$			$DS_{4,35}$	$DS_{5,35}$
36	$DS_{1,36}$	$DS_{2,36}$	$DS_{3,36}$				$DS_{4,36}$
37	$DS_{1,37}$	$DS_{2,37}$	$DS_{3,37}$				
38	$DS_{1,38}$						$DS_{2,38}$
39	$DS_{1,39}$					$DS_{2,39}$	

with fine-scale coastal features. The model results were then interpolated spatially to provide time series at the building locations.

The wind field for Katrina was developed from analyses of airborne and land-based observations, which were assimilated and transformed to a common reference condition for the inner core by using the NOAA Hurricane Research Division Wind Analysis System (H*WIND) (Powell et al., 1996, 1998). These winds were then blended with peripheral winds from the National Centers for Environmental Prediction – National Center for Atmospheric Research (NCEP-NCAR) reanalysis project (Kalnay et al., 1996), by using the Interactive Objective Kinematic Analysis (IOKA) system (Cox et al., 1995; Cardone and Cox, 2009) The resulting wind fields provide coverage of the entire Gulf of Mexico on a regular grid with snapshots every 15 min.

These wind fields were then interpolated spatially and temporally for use by the coupled SWAN + ADCIRC (Westerink et al., 2008) models. SWAN represents the wave field as a phase-averaged spectrum (Booij et al., 1999). The wave action density $N(t, \lambda, \phi, \sigma, \theta)$ evolves in time (t), geographic space (with longitudes λ and latitudes ϕ) and spectral space (with relative frequencies σ and directions θ), as governed by the action balance equation. Source terms represent wave growth by wind; energy lost due to whitecapping, depth-induced breaking, and bottom friction; and energy exchanged between spectral components due to nonlinear effects in deep and shallow water. Wave refraction and frequency shifting are represented via coupling with ADCIRC, which solves modified forms of the shallow-water equations for water levels ζ and depth-averaged currents U and V (Luettich and

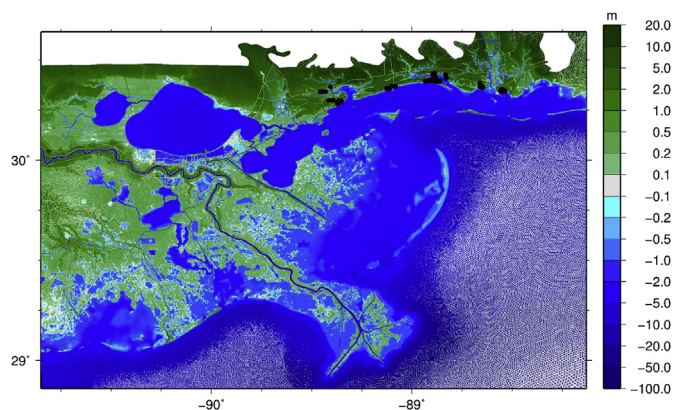


Fig. 2. Bathymetry/topography (m) of the SL16 mesh in southeastern Louisiana; the mesh extends throughout the Gulf of Mexico and the western North Atlantic Ocean (Dietrich et al., 2012b). Building locations for the analyses are shown in black dots.

Westerink, 2004; Westerink et al., 2008). These models are coupled tightly so information is passed through local memory, efficient on high-performance computing systems, and validated for hurricane wave and flooding applications along the U. S. Atlantic and Gulf coastlines (Dietrich et al., 2012b).

SWAN + ADCIRC uses unstructured meshes containing triangular finite elements of varying sizes, ranging from kilometers in open water, to hundreds of meters near the coastline and through the floodplains, and to tens of meters in the small-scale natural and man-made channels that convey surge into inland region. Katrina was simulated on the SL16 mesh (Dietrich et al., 2012b). At the building locations shown in Fig. 2, hazard attributes were interpolated spatially to provide time series of:

- Wind speed (U_{10} ; m/s), provided at an elevation of 10 m and with an averaging period of 10 min, and used as forcing to the wave and surge models;
- Significant wave height (H_S ; m), which is a statistical property computed by integrating the action density in spectral space in SWAN
- Water level (ζ ; m relative to NAVD88), computed by ADCIRC and representing the combined contributions of tides, storm surge, and wave-induced setup; and
- Water speed (U ; m/s), computed by ADCIRC and representing the depth-averaged flow at each location.

It is noted that SWAN + ADCIRC does not represent the interactions of built infrastructure with storm-driven waves and currents, but rather it represents their effects with bulk parameterizations including wind reduction due to overland roughness and canopy, and bottom friction due to land cover. Thus the computed waves and surge may not represent the finescale set-up and dissipation caused by individual structures. However, the SWAN + ADCIRC simulations are valuable because they cover large portions of the coast (including communities with devastation that may not be known a priori) and become available even during the storm events due to real-time forecasting. To quantify the uncertainties associated with these input hazard variables, we used observations of peak wave heights, water levels, and current speeds during Hurricane Katrina (2005) and the Deepwater Horizon oil spill (2010). These observations have been used previously to validate SWAN + ADCIRC predictions on this same mesh and in this same region (Dietrich et al., 2012a, 2012b). During Katrina, peak wind speeds were available at 11 buoys in open water and on the continental shelf, peak wave heights were available at 17 stations ranging from open water into the marshes of southern Louisiana, and peak water levels were available at 354 stations along the entire northern Gulf coast and near buildings and other infrastructure. To the authors' knowledge,

Table 5

Mean absolute errors and standard deviations for peak wind speeds, peak wave heights, peak water levels, and peak current speeds for SWAN and ADCIRC model.

		Katrina
Peak wind speeds	Number of stations	11
	Range of value	8.5 m/s to 28.6 m/s
	Mean absolute error	2.83 m/s
	Standard deviation	2.84 m/s
Peak wave heights	Number of stations	17
	Range of value	1.13 m–16.9 m
	Mean absolute error	1.07 m
	Standard deviation	144 m
Peak water levels	Number of stations	354
	Range of value	0.85 m–8.47 m
	Mean absolute error	0.20 m
	Standard deviation	0.3 m
Peak current speeds	Number of stations	7
	Range of value	0.85–1.28 m/s
	Mean absolute error	0.67 m/s
	Standard deviation	0.26 m/s

peak current speeds were not observed during Katrina or other recent storms in this region, but they were observed at 7 stations along the Mississippi and Alabama coasts during the oil spill. At all of these stations, the prediction uncertainties were quantified by computing mean absolute errors and standard deviations (Table 5). Given the challenges of predicting these hazard variables over such a large and complex domain, these error statistics indicate a high level of skill. They also indicate the uncertainties of these hazard variables as inputs to the fragility model.

While 10-min sustained wind speeds were used as forcing in the wave and surge models, an averaging time of 3-s is more appropriate to explain building damage (ASCE, 2010). Maximum 10-min wind speeds at each building location ($U_{10,max}$) were converted to maximum 3-s gust wind speeds ($U_{3,max}$). The Durst gust factor curve (Durst, 1960) is commonly used to convert between wind speed averaging times; however, Krayer and Marshall (1992) found that the gust factors associated with hurricane winds were higher than those associated with wind speeds from extratropical cyclones obtained from the Durst curve. The Krayer-Marshall gust factor model has been used widely for converting between averaging times of hurricane wind speeds (e.g., Vickery and Twisdale, 1995; Powell and Houston, 1996; Vickery et al., 2000). The appropriate u_i/u_{3600} gust factors for $t = 3$ s and $t = 10$ min (600 s) were obtained from the Krayer-Marshall gust curve and the maximum 3-s gust wind speed was determined at each building location in the study area.

Table 6 lists the quantitative explanatory variables (x_i) used to fit the fragility models, which are the maximum values of the time series obtained from the coupled SWAN + ADCIRC models. The maximum surge depth (D_{max}) at the centroid of each building footprint was calculated as the difference between maximum water level (ζ_{max}) and the bathymetry/topography (m) of the SL16 mesh (NAVD88) at that location.

2.3. Multicollinearity

Multicollinearity among independent variables is evaluated using

Table 6

Explanatory variables used to construct the fragility models.

x_i	Symbol	Description	Range
x_1	$U_{3,max}$	Maximum 3-s gust wind speed	[47.63–67.99] m/s
x_2	$H_{S,max}$	Maximum significant wave height	[0–3.20] m
x_3	D_{max}	Maximum surge depth above local ground	[0–7.94] m
x_4	U_{max}	Maximum water speed	[0–2.80] m/s

the variance inflation factor (VIF). The VIF for x_h is given as $VIF_h = \frac{1}{1-R_h^2}$, where R_h^2 is the coefficient of determination for a multiple regression model, considering x_h is the dependent variable and the remaining explanatory variables are independent variables. VIF_h greater than 10 indicates that x_h is almost a perfect linear combination of other explanatory variables. The multicollinearity among quantitative explanatory variables (x_h) was tested and positive correlation was found for maximum significant wave height and maximum surge depth. The coefficient of determination for the maximum significant wave height regression model was found to be $R_{HS,max}^2 = 0.968$, resulting in $VIF_{HS,max} = 15.88$. The coefficient of determination for the maximum surge depth regression model was found to be $R_{D,max}^2 = 0.963$, resulting in $VIF_{D,max} = 13.99$. With multicollinearity, one predictor variable may have reversed effect on the response variable because it overlaps with other predictors in the model. Additionally, multicollinearity may lead to both variables being insignificant when included in the same model and will inflate the standard errors of the model coefficients. With this said, $H_{S,max}$ and D_{max} are not included in the same fragility model.

3. Methodology

3.1. Fragility modeling

Binary logistic regression models, also called logit models, evaluate one dichotomy (e.g., success or failure). The generalized form of the binary logistic regression model is given as

$$\text{logit}[P] = \ln \left[\frac{P}{1-P} \right] = \alpha + \sum_{h=1}^H \beta_h x_h, \quad (1)$$

where P denotes the probability of “success,” which is defined in this study as complete failure; $\text{logit}[P]$ is the logit link function, which is equal to the natural logarithm (log) of the odds of complete failure; α is the model intercept; and β_h are model coefficients. Complete failure encompasses buildings with total structural failure, house shifted off foundation, overall structure racking, and unrepairable structural damage. These damage states are represented by WF-6 and WF-5 defined in the WF Damage Scale.

The odds of complete failure are defined as the ratio of the probability of success to its complement. Logistic regression models have been used previously to model tsunami building damage (Reese et al., 2011), hurricane power system damage (Reed et al., 2016), and hurricane building component damage (Hatzikyriakou et al., 2015).

Extending binary logistic regression models, the dependence of an ordered categorical multinomial response (e.g., DS) on discrete or continuous covariates is modeled as a series of dichotomies using the proportional odds cumulative logit model, which uses cumulative probabilities to evaluate ordered categories with the assumption that curves of the various cumulative logits are parallel (i.e., proportional odds assumption). Proportional odds cumulative logit models also have been used previously to model tsunami building damage (Charvet et al., 2014a, 2014b, 2015) and earthquake building damage (Lallemant et al., 2015).

For response variable Y with ordinal levels 1 to J (Table 2) and H explanatory variables x_1, x_2, \dots, x_H (Table 3), the log odds of response Y in level j or greater is calculated for $j \geq 2$ as

$$\text{logit}[P(Y \geq j)] = \ln \left[\frac{P(Y \geq j)}{1 - P(Y \geq j)} \right] = \alpha_j + \sum_{h=1}^H \beta_h x_h \quad \text{for } j = 2 \text{ } J \quad (2)$$

The odds of the response variable Y being in level j or greater are defined as the ratio of the probability of Y being in level j or greater $P(Y \geq j)$ to its complement. The log odds of Y being in level $j = 1$ or greater is undefined; therefore Eq. (2) results in a set of $J - 1$ equations with unique intercepts (α_j) and a common slope (β_h) for each of the H explanatory variables.

To interpret the influence of increasing hazard intensities on

damage, the hazard-specific odds ratio (OR_h) for two values of x_h (i.e. $x_{h1} x_{h2}$) with unit increase (i.e., where $x_{h2} - x_{h1} = 1$) is calculated as

$$OR_{h(1,2)} = \exp[\beta_h(x_{h2} - x_{h1})] = \frac{P(Y \geq j | X_h = x_{h1}) / P(Y < j | X_h = x_{h1})}{P(Y \geq j | X_h = x_{h2}) / P(Y < j | X_h = x_{h2})} \quad (3)$$

Given that the hazard data (x_h) are continuous variables, OR_h describes numerically the odds of a building being in a higher damage level rather than a lower damage level for each unit increase in x_h , holding all other variables constant. However, a one-unit increase in hazard intensity may not provide the most meaningful representation for OR_h , depending on the hazard. Multiple or fraction of unit increase rather than one unit increase of hazard intensities may provide a better context. For practical interpretation of MOR_h , researchers can choose a scaling factor, M_h , to represent the effect of increasing hazard intensity on the odds ratio. We see where Eq. (3) is modified to represent an M unit increase in hazard intensity. The modified odds ratio (MOR_h) for two values of x_h (i.e. $x_{h1} x_{h2}$) with M unit increase (i.e., where $x_{h2} - x_{h1} = M$) is calculated using factored model coefficients ($M_h \beta_h$). An estimate of MOR_h is given as $\exp(M_h * \hat{\beta}_h)$, while 95% lower (LCI) and upper (UCI) confidence intervals ($MOR_{h,CI_{95\%}}$) of the MOR_h is given as $\exp[M_h(\hat{\beta}_h \pm 1.96 * SE(\hat{\beta}_h))]$. Where $\hat{\beta}_h$ are the estimated model coefficients, and $SE(\hat{\beta}_h)$ is the standard error of the estimated model coefficients $\hat{\beta}_h$.

To reflect the effect of one hazard intensity on damage based on the value of another hazard intensity, the interaction between hazards is represented as the sum of hazard product terms “ $x_h x_q$ ”. The log odds of response Y in level j or greater is calculated for $j \geq 2$ as

$$\text{logit}[P(Y \geq j)] = \ln \left[\frac{P(Y \geq j)}{1 - P(Y \geq j)} \right] = \alpha_j + \sum_{h=1}^H \beta_h x_h + \sum_{1 \leq h < q \leq H} \beta_{hq} x_h x_q \quad \text{for } j = 2 \text{ } J \quad (4)$$

where β_{hq} are the coefficients of two hazard interaction terms. Variables x_h and x_q are two hazard terms where $q > h$. All model coefficients are estimated using Maximum Likelihood Estimation (MLE).

The estimated probability of Y being in or exceeding level j is calculated for $j \geq 2$ as

$$P(Y \geq j) = \frac{\exp \left(\alpha_j + \sum_{h=1}^H \beta_h x_h + \sum_{1 \leq h < q \leq H} \beta_{hq} x_h x_q \right)}{1 + \exp \left(\alpha_j + \sum_{h=1}^H \beta_h x_h + \sum_{1 \leq h < q \leq H} \beta_{hq} x_h x_q \right)} \quad \text{for } j = 2 \text{ } J \quad (5)$$

The estimated probability of Y being in or exceeding the first level ($j = 1$) is equal to one. Solving for $P(Y = j)$, the estimated probability that the DS falls into a specific level, is calculated for levels $j \leq J - 1$ as $P(Y = j) = P(Y \geq j) - P(Y \geq j + 1)$ for $j \leq J - 1$ (6)

The estimated probability that the DS falls into level J is equal to the probability of being in or exceeding level J , as calculated in Eq. (5). With interaction terms, interpretation of the odds ratios becomes more involved since the influence of increasing hazard intensities on damage now depends on levels of other hazards.

3.2. Model fitting and evaluation

SAS software (Version 9.4) is used to fit the fragility model. For each Model (n), two models with three hazard variables were fitted based on Eq. (2), resulting in a total of 78 models. These models are described with (x_1, x_2 , and x_4), and (x_1, x_3 , and x_4) hazard variables. Four criteria are used to evaluate the fit and prediction of the 78 models. The first two are of the form of rejection criteria for screening purposes, while the last two are qualitative criteria used to further narrow the net of the

non-rejected models.

Satisfaction of model requirements (proportional odds assumption and goodness of fit). For proportional odds cumulative models, the proportional odds assumption assumes that the coefficients for each hazard predictor must be equal across all DS levels and is tested using the chi-square test. For the logistic regression model, the Hosmer and Lemeshow test is used to assess goodness of fit based on the chi-square test. The data are grouped based on a partitioning of the estimated probabilities, then the test compares the observed and fitted counts of the groups. Any model with chi-square p -values < 0.05 is rejected.

Statistical significance of model parameters. At least one main hazard effect must be significant or the model is rejected.

Reasonableness of response variable model. Once models that pass the rejection criteria are identified, this subjective parameter is used to evaluate the most reasonable model(s) for prediction. Models with high prediction accuracy but with unreasonable response variable grouping (e.g., minor damage falls into the same level as severe damage) are considered less reasonable models for damage prediction.

Balance between CCR and class error. Once models that pass the rejection criteria are identified, this criterion is used to evaluate the most reasonable model(s) for prediction. Models with high prediction accuracy (i.e., high value of CCR) but with high class error are considered less reasonable models for damage prediction.

Among the 78 models, models satisfying Criterion 1 are evaluated for Criterion 2. Models satisfying the two rejection criteria are then reevaluated based on Eq. (4) to include hazard interaction terms and are reevaluated based on the two rejection criteria. Models with interaction terms are described as 1) one model with three hazard variables and three hazard interaction terms, 2) three models with three hazard variables and two hazard interaction terms, and 3) three models with three hazard variables and one hazard interaction term.

3.3. Model validation

Prediction accuracy for logistic regression and proportional odds cumulative logit models is often evaluated using external cross-validation. When external test data are not available, k -fold cross-validation is one of the most widely used approaches to assess external prediction. In k -fold cross-validation, the data are partitioned into k subsamples, with $k-1$ subsamples used for fitting the model, while the remaining one is used for model validation. The process is cycled through all partitions, each in turn predicting the left out partition using the model that has been trained on all other partitions. Due to sample size considerations, our research implements a special case of k -fold cross-validation, namely leave-one-out cross-validation (LOOCV), where k is equal to the number of observations (N) in the dataset. Models that satisfied the rejection criteria are fitted N times, with one observation left out at each fit. For each fit, the predicted DS ($\hat{D}S$) for every left out observation is estimated as follows:

For the proportional odds cumulative logit models, the estimated probabilities that a DS fall into specific level J is calculated based on Eq. (6), and then the DS corresponding to the highest estimated probability is assigned as the predicted DS ($\hat{D}S$). The process is repeated for every left out observation.

For the logistic regression model, the estimated probability of complete failure is calculated as

$$P = \frac{\exp(\alpha + \sum_{h=1}^H \beta_h x_h)}{1 + \exp(\alpha + \sum_{h=1}^H \beta_h x_h)}$$
. If the estimated probability of complete failure is greater than 0.5, complete failure is assigned as the predicted DS ($\hat{D}S$), otherwise no complete failure is assigned. The process is repeated for every left out observation.

For every satisfactory model and after assigning the predicted DS ($\hat{D}S$) for every left out observation, an error matrix with N total observations is constructed. Rows (d) of the matrix represent the frequency (z) of observed DS, while columns (c) represent the frequency of predicted DS ($\hat{D}S$), summed across the N left out observations of the

model. The percentage of correctly classified damage states, expressed as the cross-classification rate (CCR; Eq. (7)), is calculated as

$$CCR = \frac{\sum_{c=1}^C z_{cc}}{\sum_{c=1}^C \sum_{d=1}^D z_{cd}}, \quad (7)$$

where z_{cc} are observations along the diagonal of the error matrix, and z_{cd} are all observations in the error matrix. The percentage of each misclassified DS, expressed as class error (CE), is calculated as $CE = 1 - \frac{z_{cc}}{\sum_{c=1}^C z_{cd}}$.

4. Results and discussion

4.1. Fragility fitting

Based on Eq. (2), Models 8, 9, 10, 25, 26, and 27 with hazard variables $U_{3,max}$, $H_{s,max}$, and U_{max} and Model 38 with hazard variables $U_{3,max}$, D_{max} , and U_{max} satisfied the two rejection criteria, while the remainder of the models failed to meet the first rejection criterion and were not further tested for Criterion 2. When hazard interaction terms were included (Eq. (4)), no interaction terms were found to be significant. Therefore, none of the models with hazard interaction terms satisfied the two rejection criteria and were therefore removed from further consideration.

Table 7 contains the estimated coefficients, standard error, p -value, factored model coefficients, MOR_h , and LCI and UCI of $MOR_h CI_{95\%}$ for models that met the rejection criteria. Factored model coefficients, MOR_h , and $MOR_h CI_{95\%}$ were calculated using $M_{U_{3,max}} = 4.5$ (m/s), $M_{H_{s,max}} = 0.3$ (m), $M_{D_{max}} = 1$ (m), and $M_{U_{max}} = 0.5$ (m/s).

For all DS models, the only statistically significant hazard variable was the maximum significant wave height, while maximum 3-s gust wind speed and maximum water speed were not found to significantly affect damage. The results show that the primary DS determinant for buildings subjected to wind, wave, and water speed is the maximum significant wave height. However, the p -value (0.0522) of the maximum water speed coefficient ($\hat{\beta}_3$) is on the border of the significance level ($\alpha = 0.05$) for Model 10 and very close to the border of the significance level for Models 8, 9, and 25, which indicates that maximum water speed may have an effect on increasing damage. Kennedy et al. (2010), Tomiczek et al. (2014a), and Tomiczek et al. (2017) also found that significant wave height significantly contributes to damage and should be considered in the development of fragility models. The average odds for maximum significant wave height of the six DS models is 3.57. This is interpreted as: for every 0.3 m (0.98 ft) increase in maximum significant wave height, the odds of being in a higher DS are 3.57 times greater (257% increase in odds), holding all other variables constant. Among all DS models, the odds for maximum water speed were the highest for Model 10, which is interpreted as: for every 0.5 m/s (1.64 ft/s) increase in maximum water speed, the odds of being in a higher DS are 2.05 times greater (105% increase in odds).

For Model 38, which predicts binary complete failure/non-complete failure, all three hazard variables were statistically significant. The results show that the complete failure potential of buildings subjected to wind, surge, and water speed are significantly affected by all three hazards. As any of the hazard variables increase, the odds of complete failure increase. Tomiczek et al. (2014a) and Tomiczek et al. (2017) also found that water speed contributes significantly to complete failure and damage and should be considered in the development of fragility models. However, these authors excluded wind speed from their analyses without statistical testing. Their assumption was based on the fact that Hurricanes Ike (2009) and Sandy (2012) had wind speeds lower than common damage initiation thresholds. Similar to Hurricanes Ike and Sandy, Hurricane Katrina was an event with lower wind speeds; however, the maximum 3-s gust wind speed was found to be a significant contributor to complete failure. Interpretation of the odds shows that, holding all other variables constant:

Table 7
Parameter estimates, standard error, *p*-value, MOR_h and MOR_hCI_{95%} for models satisfying rejection criteria.

Model	Coefficient	Parameter	Estimated	Std. Error	<i>p</i> -value	$M_{\beta_h}\hat{\beta}_h$	MOR _h	MOR _h CI _{95%}		
								LCI	UCI	
8	$\hat{\alpha}_2$	Intercept 2	-7.66	1.55	< 0.0001	^a	-	-	-	-
	$\hat{\alpha}_3$	Intercept 3	-8.08	1.55	< 0.0001	^a	-	-	-	-
	$\hat{\alpha}_4$	Intercept 4	-8.5	1.55	< 0.0001	^a	-	-	-	-
	$\hat{\beta}_1$	$U_{3,max}$	0.05	0.03	0.0722		0.23	1.26	0.96	1.63
	$\hat{\beta}_2$	$H_{S,max}$	4.13	0.32	< 0.0001	^a	1.24	3.46	2.86	4.17
	$\hat{\beta}_3$	U_{max}	1.11	0.66	0.0938		0.56	1.75	0.91	3.33
9	$\hat{\alpha}_2$	Intercept 2	-7.63	1.55	< 0.0001	^a	-	-	-	-
	$\hat{\alpha}_3$	Intercept 3	-8.47	1.55	< 0.0001	^a	-	-	-	-
	$\hat{\beta}_1$	$U_{3,max}$	0.05	0.03	0.0750		0.23	1.26	0.96	1.63
	$\hat{\beta}_2$	$H_{S,max}$	4.12	0.32	< 0.0001	^a	1.24	3.46	2.85	4.15
	$\hat{\beta}_3$	U_{max}	1.16	0.67	0.0829		0.58	1.79	0.93	3.44
	10	$\hat{\alpha}_2$	Intercept 2	-7.77	1.59	< 0.0001	^a	-	-	-
$\hat{\alpha}_3$		Intercept 3	-8.19	1.59	< 0.0001	^a	-	-	-	-
$\hat{\beta}_1$		$U_{3,max}$	0.05	0.03	0.0665		0.23	1.26	0.96	1.63
$\hat{\beta}_2$		$H_{S,max}$	4.02	0.33	< 0.0001	^a	1.21	3.35	2.75	4.06
$\hat{\beta}_3$		U_{max}	1.43	0.74	0.0522		0.72	2.05	0.99	4.22
25		$\hat{\alpha}_2$	Intercept 2	0.28	1.45	0.8494		-	-	-
	$\hat{\alpha}_3$	Intercept 3	-7.45	1.5	< 0.0001	^a	-	-	-	-
	$\hat{\alpha}_4$	Intercept 4	-7.9	1.5	< 0.0001	^a	-	-	-	-
	$\hat{\alpha}_5$	Intercept 5	-8.3	1.5	< 0.0001	^a	-	-	-	-
	$\hat{\beta}_1$	$U_{3,max}$	0.04	0.03	0.1016		0.18	1.2	0.92	1.56
	$\hat{\beta}_2$	$H_{S,max}$	4.22	0.32	< 0.0001	^a	1.27	3.56	2.94	4.28
26	$\hat{\beta}_3$	U_{max}	1.24	0.67	0.0660		0.62	1.86	0.96	3.58
	$\hat{\alpha}_2$	Intercept 2	0.06	1.56	0.9674		-	-	-	-
	$\hat{\alpha}_3$	Intercept 3	-8.39	1.66	< 0.0001	^a	-	-	-	-
	$\hat{\alpha}_4$	Intercept 4	-8.82	1.66	< 0.0001	^a	-	-	-	-
	$\hat{\beta}_1$	$U_{3,max}$	0.05	0.03	0.0875		0.23	1.26	0.96	1.63
	$\hat{\beta}_2$	$H_{S,max}$	4.39	0.35	< 0.0001	^a	1.32	3.74	3.04	4.59
27	$\hat{\beta}_3$	U_{max}	0.93	0.69	0.1797		0.47	1.6	0.81	3.13
	$\hat{\alpha}_2$	Intercept 2	-0.12	1.75	0.9470		-	-	-	-
	$\hat{\alpha}_3$	Intercept 3	-9	1.85	< 0.0001	^a	-	-	-	-
	$\hat{\beta}_1$	$U_{3,max}$	0.05	0.03	0.1185		0.23	1.26	0.96	1.63
	$\hat{\beta}_2$	$H_{S,max}$	4.5	0.38	< 0.0001	^a	1.35	3.86	3.09	4.59
	$\hat{\beta}_3$	U_{max}	0.89	0.72	0.2178		0.45	1.57	0.81	3.13
38	$\hat{\alpha}$	Intercept	-18.00	1.92	< 0.0001	^a	-	-	-	-
	$\hat{\beta}_1$	$U_{3,max}$	0.22	0.03	< 0.0001	^a	0.99	2.69	2.07	3.51
	$\hat{\beta}_2$	D_{max}	0.99	0.10	< 0.0001	^a	0.99	2.69	1.27	1.43
	$\hat{\beta}_3$	U_{max}	2.32	0.69	0.0008	^a	1.16	3.19	1.62	6.27

^a Significant at $\alpha = 0.05$.

- for every 4.5 m/s (10.07 mph) increase in maximum 3-s gust wind speed, the odds of complete failure are 2.69 times greater (169% increase in odds)
- for every 0.5 m/s (1.64 ft/s) increase in maximum water speed, the odds of complete failure are 3.19 times greater (219% increase)
- for every 1 m (3.28 ft) increase in maximum surge depth, the odds of complete failure are 2.69 times greater (169% increase in odds)

4.2. Model validation and evaluation

LOOCV error matrices for the seven models that satisfied the rejection criteria are provided in Table 8. Rows of the tables represent the frequency of observed DS, while columns represent the frequency of predicted DS ($\hat{D}S$). The *n* subscript in the predicted DS ($\hat{D}S$) represents the corresponding model number.

The results show that the overall model prediction accuracies are high, with CCR ranging from 81% to 87%, although individual DS or several DS have high CE (> 50%). High CE were found for all DS levels with few observations.

4.2.1. DS fragility models

Model 8 has reasonable grouping of DS; however, the model has two DS with high CE. Models 25 and 26 have three and two DS with high CE, respectively, as well as unreasonable groupings of DS, where DS_{2,25} ranges from minor damage to severe damage and DS_{2,26} ranges from minor damage to very severe damage. Model 27 has the highest prediction accuracy (85%); however, DS_{2,27} has an unreasonable grouping, ranging from minor damage to partial complete failure and DS_{1,27} has a high CE (75%). Because of the number of DS with high CE and unreasonable groupings of DS, Models 8, 25, 26, and 27 are excluded from consideration, while Models 9 and 10 are evaluated further.

Model 10 has 2% higher prediction accuracy and 4% higher CE than Model 9. However, Model 10 has a more reasonable response variable grouping than Model 9, where DS_{3,10} represents partial complete failure and complete failure, while DS_{2,9} represents very severe damage and partial complete failure. Additionally, the *p*-value (0.0522) for the maximum water speed coefficient ($\hat{\beta}_3$) in Model 10 is on the border of the significance level ($\alpha = 0.05$). Therefore, Model 10 is chosen as the more reasonable predictive fragility model to predict the probability of being in or exceeding DS_{2,10} and DS_{3,10} as a function of maximum 3-s

Table 8
Observed vs. predicted model error matrices, CE, and CCR for non-rejected models.

DS _{j,n}	DŜ _{1,n}	DŜ _{2,n}	DŜ _{3,n}	DŜ _{4,n}	DŜ _{5,n}	Observed Sum	CE	CCR
DS _{1,8}	375	16	7	22	–	420	11%	81%
DS _{2,8}	21	5	1	18	–	45	89%	
DS _{3,8}	18	2	1	21	–	42	98%	
DS _{4,8}	23	8	8	320	–	359	11%	
DS _{1,9}	370	21	29	–	–	420	12%	81%
DS _{2,9}	41	13	33	–	–	87	85%	
DS _{3,9}	21	18	320	–	–	359	11%	
DS _{1,10}	370	17	33	–	–	420	12%	83%
DS _{2,10}	20	5	20	–	–	45	89%	
DS _{3,10}	42	19	340	–	–	401	15%	
DS _{1,25}	0	4	0	0	0	4	100%	81%
DS _{2,25}	1	380	5	7	23	416	9%	
DS _{3,25}	0	22	3	1	19	45	93%	
DS _{4,25}	0	19	3	1	19	42	98%	
DS _{5,25}	1	27	7	4	320	359	11%	
DS _{1,26}	1	3	0	0	–	4	75%	85%
DS _{2,26}	1	420	6	34	–	461	9%	
DS _{3,26}	0	21	2	19	–	42	95%	
DS _{4,26}	1	38	3	317	–	359	12%	
DS _{1,27}	1	3	0	–	–	4	75%	85%
DS _{2,27}	1	440	57	–	–	498	12%	
DS _{3,27}	1	65	298	–	–	364	18%	
DS _{1,38}	450	57	–	–	–	507	11%	87%
DS _{2,38}	58	301	–	–	–	359	16%	

Note: - indicates error terms are not applicable due to the number of damage levels j for model n.

gust wind speed, maximum significant wave height, and maximum water speed. There is not one specific rule that can be used to select a “final” model between Model 9 and Model 10. Since both models satisfy the rejection criteria, the choice of the model is subjective. Both models are reasonable to be used as a predictive fragility model.

The estimated probability of being in or exceeding DS_{2,10} and DS_{3,10}, respectively, as a function of maximum 3-s gust wind speed, maximum significant wave height, and maximum water speed is estimated as

$$\text{logit}[P(Y \geq DS_{2,10})] = -7.77 + 0.05*U_{3,max} + 4.02*H_{S,max} + 1.43*U_{max}, \text{ and} \tag{8}$$

$$\text{logit}[P(Y \geq DS_{3,10})] = -8.19 + 0.05*U_{3,max} + 4.02*H_{S,max} + 1.43*U_{max} \tag{9}$$

Fig. 3a) and b) show fragility surfaces for Model 10 as a function of maximum significant wave height and maximum water speed considering maximum 3-s wind speed of 62 m/s.

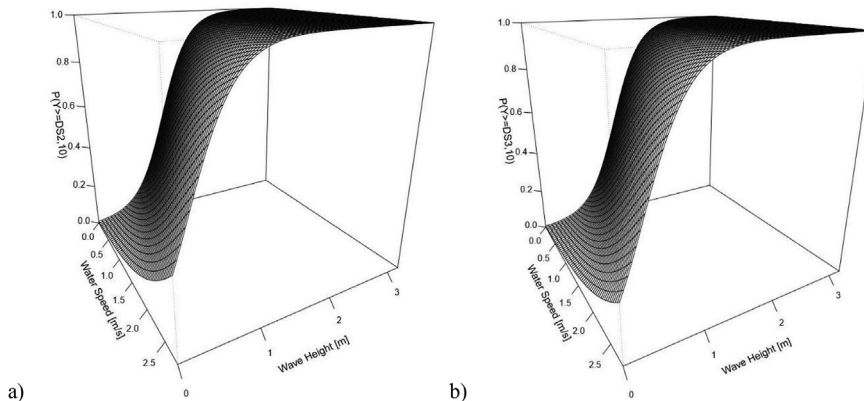


Fig. 3. Probability of being in or exceeding a) DS_{2,10} and b) DS_{3,10} as a function of maximum significant wave height and maximum water speed.

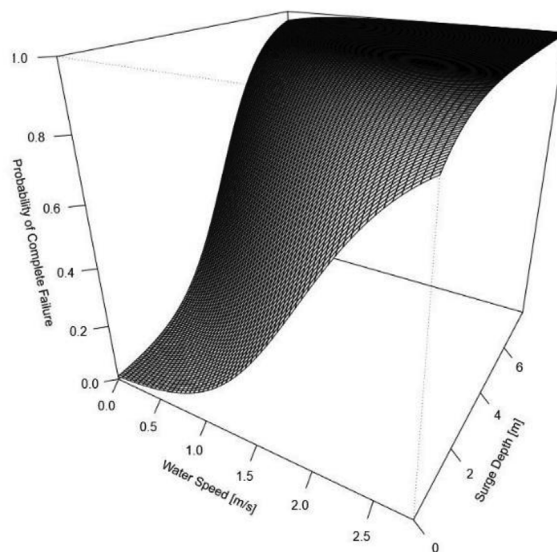


Fig. 4. Probability of complete failure as a function of maximum surge depth and maximum water speed.

4.2.2. Complete failure fragility model

Model 38 predicts probability of complete failure as a function of maximum 3-s gust wind speed, maximum surge depth, and maximum water speed with 87% prediction accuracy. No high CE values are shown due to large sample sizes. The estimated probability of complete failure ($Y \geq DS_{38,2}$) as a function of maximum 3-s gust wind speed, maximum surge depth, and maximum water speed is given as

$$\text{logit}[P(Y \geq DS_{38,2})] = -18 + 0.22*U_{3,max} + 0.99*D_{max} + 2.32*U_{max} \tag{10}$$

Fig. 4 shows the fragility surface for Model 38 as a function of maximum surge depth and maximum water speed considering maximum 3-s wind speed of 62 m/s.

4.2.3. Study limitations

Limitations of this approach are that the results have been derived as a function of the range of hazard values experienced only during Hurricane Katrina in coastal Mississippi. While the damage reconnaissance included multiple communities with increasing distance from the hurricane track, and thus decreasing hazard levels, the wind speeds ranged between 48 and 68 m/s. Because pressure is proportional to the square of the wind speed and older roof cover damage may begin around 42–48 m/s, the wind speeds experienced in Hurricane Katrina did not cause substantial damage, which limits the applicability of this model to more intense wind events. Uncertainty resulting from using

the gust factor from Kraymer-Marshall curve was not considered when converting maximum 10-min wind speed to maximum 3-s gust wind speed. Additionally, because of the limited data range available for model development, the fragility models are valid only within the ranges given in Table 6. The developed fragility models are limited to building type rather than to particular regions. The developed fragility models can be applied to buildings in any region as long as the buildings are of the same type as the buildings defined in this study area and are subjected to the range of hazard intensities defined in Table 6. A limitation of the underlying building and damage data is that a specified sampling technique was not implemented during the original field data collection and required sample sizes in each DS were not considered.

5. Summary and conclusions

While the results of this study are specific to the U.S. Gulf Coast, the statistical concept behind the developed methodology is applicable to any building type, study area, and hazard type around the globe. The developed methodology is useful for researchers, insurance companies, and model developers who have access to datasets describing single-family home damage and performance during extreme events (e.g. hurricane, flood) to aid the development of multi-hazard building fragility models. Most importantly, the methodology and results are useful for users who rely on loss functions for risk assessment and catastrophic models used by insurance companies. The use of the cross validation approach validates the prediction of the models and insures that the models are applicable to buildings in the current study area and other areas of similar construction. The authors advocate that in the future the developed models are evaluated based on other datasets and that a comparison using cross validation is conducted.

Physical damage to residential buildings from hurricane wind, wave, and storm surge hazards was statistically modeled and hazard attributes that contribute significantly to damage and complete failure were determined. The proportional odds cumulative logit model was used to estimate the probability of damage being in or exceeding ordered categorical DS as a function of maximum 3-s gust wind speed, maximum significant wave height, and maximum water speed. The logistic regression model was used to estimate probability of complete failure as a function of maximum 3-s gust wind speed, maximum surge depth, and maximum water speed. The findings of this paper are:

The proportional odds cumulative logit model showed high accuracy in estimating the probability of being in or exceeding categorical ordered DS as a function of multiple hurricane hazards.

The logistic regression model showed high accuracy in estimating the probability of complete failure as a function of multiple hurricane hazards.

Maximum significant wave height was found to be the only significant predictor of damage for the ordered categorical DS models, while maximum 3-s gust wind speed, maximum water speed, and maximum surge depth were found to be significant predictors for complete failure.

Maximum water speed was found to be on the border of the significance level for one proportional odds cumulative logit model and very close to the significance level for three proportional odds cumulative logit models.

High collinearity was found between maximum surge depth and maximum significant wave height, resulting in VIF greater than 10. Therefore, models were constructed without the consideration of $H_{S,max}$ and D_{max} in the same fragility model.

Low sample numbers in WF0, WF1, WF4, and WF5 resulted in high CE for these DS and any response variable groupings of these DS.

Application of proportional odds cumulative logit and logistic regression models confirm the effectiveness of statistical models for development of multi-hazard hurricane fragility surfaces and identification of hazard variables that significantly contribute to damage and

complete failure.

Acknowledgments

The authors gratefully acknowledge funding from the Louisiana Board of Regents Graduate Fellowship in Engineering Grant # LEQSF (2008-13)GF-01, the Donald W. Clayton Graduate PhD Assistantship in Engineering, and the Chevron Engineering Graduate Student Fellowship. Hurricane Katrina reconnaissance videos were provided by MCEER (<http://www.buffalo.edu/mceer.html>).

Appendix A. Supplementary data

Supplementary data related to this article can be found at <https://doi.org/10.1016/j.coastaleng.2019.04.008>.

References

- Adams, B.J., Huyck, C., Mio, M., Cho, S., Eguchi, R.T., Womble, A., Mehta, K., 2004. Streamlining post-disaster data collection and damage assessment, using VIEWS (visualizing impacts of earthquakes with satellites) and VRS (virtual reconnaissance system). In: Paper Presented at the Proceedings of 2nd International Workshop on Remote Sensing for Post-Disaster Response, Newport Beach, California.
- ASCE, 2010. Minimum Design Loads for Buildings and Other Structures. American Society of Civil Engineers, Reston, VA.
- Barbato, M., Petrini, F., Unnikrishnan, V.U., Ciampoli, M., 2013. Performance-based hurricane engineering (PBHE) framework. Struct. Saf. 45, 24–35. <http://10.1016/j.strusafe.2013.07.002>.
- Booij, N., Ris, R., Holthuijsen, L.H., 1999. A third-generation wave model for coastal regions: 1. Model description and validation. J. Geophys. Res.: Oceans 104 (C4), 7649–7666. <http://10.1029/98JC02622>.
- Bunya, S., Dietrich, J.C., Westerink, J., Ebersole, B., Smith, J., Atkinson, J., Jensen, R., Resio, D., Luettich, R., Dawson, C., 2010. A high-resolution coupled riverine flow, tide, wind, wind wave, and storm surge model for southern Louisiana and Mississippi. Part I: model development and validation. Mon. Weather Rev. 138 (2), 345–377. <http://doi.org/10.1175/2009MWR2906.1>.
- Cardone, V., Cox, A., 2009. Tropical cyclone wind field forcing for surge models: critical issues and sensitivities. Nat. Hazards 51 (1), 29–47. <http://doi.org/10.1007/s11069-009-9369-0>.
- Charvet, I., Ioannou, I., Rossetto, T., Suppasri, A., Imamura, F., 2014a. Empirical fragility assessment of buildings affected by the 2011 Great East Japan tsunami using improved statistical models. Nat. Hazards 73 (2), 951–973. <http://doi.org/10.1007/s11069-014-1118-3>.
- Charvet, I., Suppasri, A., Imamura, F., 2014b. Empirical fragility analysis of building damage caused by the 2011 Great East Japan tsunami in Ishinomaki city using ordinal regression, and influence of key geographical features. Stoch. Environ. Res. Risk Assess. 28 (7), 1853–1867. <https://doi.org/10.1007/s00477-014-0850-2>.
- Charvet, I., Suppasri, A., Kimura, H., Sugawara, D., Imamura, F., 2015. A multivariate generalized linear tsunami fragility model for Kesennuma City based on maximum flow depths, velocities and debris impact, with evaluation of predictive accuracy. Nat. Hazards 79 (3), 2073–2099. <https://doi.org/10.1007/s11069-015-1947-8>.
- Choine, M.N., O'Connor, A., Gehl, P., D'Ayala, D., García-Fernández, M., Jiménez, M.-J., Gavin, K., Van Gelder, P., Salceda, T., Power, R., 2015. A multi hazard risk assessment methodology accounting for cascading hazard events. In: Paper Presented at the Proceedings of 12th International Conference on Applications of Statistics and Probability in Civil Engineering (ICASP12), Vancouver, Canada.
- Cox, A., Greenwood, J., Cardone, V., Swail, V., 1995. An interactive objective kinematic analysis system. In: Paper Presented at the Proceedings of Fourth International Workshop on Wave Hindcasting and Forecasting, Downsview, Ontario.
- Crandell, J.H., 1998. Statistical assessment of construction characteristics and performance of homes in Hurricanes Andrew and Opal. J. Wind Eng. Ind. Aerod. 77–78, 695–701. [https://doi.org/10.1016/S0167-6105\(98\)00184-6](https://doi.org/10.1016/S0167-6105(98)00184-6).
- Curtis, A., Duval-Diop, D., Novak, J., 2010. Identifying spatial patterns of recovery and abandonment in the post-Katrina Holy Cross neighborhood of New Orleans. Cartogr. Geogr. Inf. Sci. 37 (1), 45–56. <https://doi.org/10.1559/152304010790588043>.
- Curtis, A., Mills, J.W., Kennedy, B., Fotheringham, S., McCarthy, T., 2007a. Understanding the geography of post-traumatic stress: an academic justification for using a spatial video acquisition system in the response to Hurricane Katrina. J. Contingencies Crisis Manag. 15 (4), 208–219. <https://doi.org/10.1111/j.1468-5973.2007.00522.x>.
- Curtis, A., Mills, J.W., Leitner, M., 2007b. Katrina and vulnerability: the geography of stress. J. Health Care Poor Underserved 18 (2), 315–330. <https://10.1353/hpu.2007.0029>.
- Dietrich, J., Trahan, C., Howard, M., Fleming, J., Weaver, R., Tanaka, S., Yu, L., Luettich Jr., R., Dawson, C., Westerink, J., 2012a. Surface trajectories of oil transport along the northern coastline of the Gulf of Mexico. Cont. Shelf Res. 41, 17–47. <https://doi.org/10.1016/j.csr.2012.03.015>.
- Dietrich, J.C., Bunya, S., Westerink, J., Ebersole, B., Smith, J., Atkinson, J., Jensen, R., Resio, D., Luettich, R., Dawson, C., 2010. A high-resolution coupled riverine flow, tide, wind, wind wave, and storm surge model for southern Louisiana and Mississippi.

- Part II: synoptic description and analysis of Hurricanes Katrina and Rita. *Mon. Weather Rev.* 138 (2), 378–404. <http://doi.org/10.1175/2009MWR2907.1>.
- Dietrich, J.C., Tanaka, S., Westerink, J.J., Dawson, C., Luettich Jr., R., Zijlema, M., Holthuijsen, L.H., Smith, J., Westerink, L., Westerink, H., 2012b. Performance of the unstructured-mesh, SWAN+ ADCIRC model in computing hurricane waves and surge. *J. Sci. Comput.* 52 (2), 468–497. <http://doi.org/10.1007/s10915-011-9555-6>.
- Durst, C., 1960. Wind speeds over short periods of time. *Meteorol. Mag.* 89, 181–186.
- Friedland, C.J., Levitan, M.L., 2009. Loss-consistent categorization of hurricane wind and storm surge damage for residential structures. In: *Paper Presented at the Proceedings of the 11th Americas Conference on Wind Engineering, San Juan, Puerto Rico*.
- Fritz, H.M., Blount, C., Sokolowski, R., Singleton, J., Fuggle, A., McAdoo, B.G., Moore, A., Grass, C., Tate, B., 2008. Hurricane Katrina storm surge reconnaissance. *J. Geotech. Geoenviron. Eng.* 134 (5), 644–656. [https://doi.org/10.1061/\(ASCE\)1090-0241\(2008\)134:5\(644\)](https://doi.org/10.1061/(ASCE)1090-0241(2008)134:5(644)).
- Geisser, S., 1975. The predictive sample reuse method with applications. *J. Am. Stat. Assoc.* 70 (350), 320–328. <https://doi.org/10.2307/2285815>.
- Hatzikyriakou, A., 2017. *Vulnerability and Hazard Modeling for Coastal Flooding Due to Storm Surge* (PhD Dissertation). Princeton University, Princeton, New Jersey.
- Hatzikyriakou, A., Lin, N., 2018. Assessing the vulnerability of structures and residential communities to storm surge: an analysis of flood impact during Hurricane Sandy. *Front. Built Environ.* 4 (4). <https://doi.org/10.3389/fbuil.2018.00004>.
- Hatzikyriakou, A., Lin, N., Gong, J., Xian, S., Hu, X., Kennedy, A., 2015. Component-based vulnerability analysis for residential structures subjected to storm surge impact from Hurricane Sandy. *Nat. Hazards Rev.* 17 (1). [https://doi.org/10.1061/\(ASCE\)NH.1527-6996.0000205](https://doi.org/10.1061/(ASCE)NH.1527-6996.0000205).
- Kalnay, E., Kanamitsu, M., Kistler, R., Collins, W., Deaven, D., Gandin, L., Iredell, M., Saha, S., White, G., Woollen, J., 1996. The NCEP/NCAR 40-year reanalysis project. *Bull. Am. Meteorol. Soc.* 77 (3), 437–471. [https://doi.org/10.1175/1520-0477\(1996\)077<0437:TNYRP>2.0.CO;2](https://doi.org/10.1175/1520-0477(1996)077<0437:TNYRP>2.0.CO;2).
- Kameshwar, S., Padgett, J.E., 2018. Fragility and resilience indicators for portfolio of oil storage tanks subjected to hurricanes. *J. Infrastruct. Syst.* 24 (2), 04018003. [https://doi.org/10.1061/\(ASCE\)IS.1943-555X.0000418](https://doi.org/10.1061/(ASCE)IS.1943-555X.0000418).
- Kappes, M., Keiler, M., von Elverfeldt, K., Glade, T., 2012a. Challenges of analyzing multi-hazard risk: a review. *Nat. Hazards* 64 (2), 1925–1958. <http://doi.org/10.1007/s11069-012-0294-2>.
- Kappes, M., Papathoma-Köhle, M., Keiler, M., 2012b. Assessing physical vulnerability for multi-hazards using an indicator-based methodology. *Appl. Geogr.* 32 (2), 577–590. <https://doi.org/10.1016/j.apgeog.2011.07.002>.
- Kennedy, A., Rogers, S., Sallenger, A., Gravois, U., Zachry, B., Dosa, M., Zarama, F., 2010. Building destruction from waves and surge on the bolivar peninsula during hurricane Ike. *J. Waterw. Port, Coast. Ocean Eng.* 137 (3), 132–141. [https://doi.org/10.1061/\(ASCE\)WW.1943-5460.0000061](https://doi.org/10.1061/(ASCE)WW.1943-5460.0000061).
- Khanduri, A., Morrow, G., 2003. Vulnerability of buildings to windstorms and insurance loss estimation. *J. Wind Eng. Ind. Aerod.* 91 (4), 455–467. [https://doi.org/10.1016/S0167-6105\(02\)00408-7](https://doi.org/10.1016/S0167-6105(02)00408-7).
- Koshimura, S., Namegaya, Y., Yanagisawa, H., 2009. Tsunami fragility: a new measure to identify tsunami damage. *J. Disaster Res.* 4 (6), 479–488. <https://doi.org/10.20965/jdr.2009.p0479>.
- Krayer, W.R., Marshall, R.D., 1992. Gust factors applied to hurricane winds. *Bull. Am. Meteorol. Soc.* 73 (5), 613–618. [https://doi.org/10.1175/1520-0477\(1992\)073<0613:GFATHW>2.0.CO;2](https://doi.org/10.1175/1520-0477(1992)073<0613:GFATHW>2.0.CO;2).
- Lallemant, D., Kiremidjian, A., Burton, H., 2015. Statistical procedures for developing earthquake damage fragility curves. *Earthq. Eng. Struct. Dyn.* <https://doi.org/10.1002/eqe.2522>.
- Lee, K.H., Rosowsky, D.V., 2005. Fragility assessment for roof sheathing failure in high wind regions. *Eng. Struct.* 27 (6), 857–868. <https://doi.org/10.1016/j.engstruct.2004.12.017>.
- Lee, K.H., Rosowsky, D.V., 2006. Fragility analysis of woodframe buildings considering combined snow and earthquake loading. *Struct. Saf.* 28 (3), 289–303. <http://doi.org/10.1016/j.strusafe.2005.08.002>.
- Li, Y., Ellingwood, B.R., 2009a. Framework for multihazard risk assessment and mitigation for wood-frame residential construction. *J. Struct. Eng.* 135 (2), 159–168. [https://doi.org/10.1061/\(ASCE\)0733-9445\(2009\)135:2\(159\)](https://doi.org/10.1061/(ASCE)0733-9445(2009)135:2(159)).
- Li, Y., Ellingwood, B.R., 2009b. Risk-based decision-making for multi-hazard mitigation for wood-frame residential construction. *Aust. J. Struct. Eng.* 9 (1), 17. <https://doi.org/10.1080/13287982.2009.11465006>.
- Li, Y., van de Lindt, J.W., 2012. Loss-based formulation for multiple hazards with application to residential buildings. *Eng. Struct.* 38 (0), 123–133. <https://doi.org/10.1016/j.engstruct.2012.01.006>.
- Li, Y., van de Lindt, J.W., Dao, T., Bjarnadottir, S., Ahuja, A., 2011. Loss analysis for combined wind and surge in hurricanes. *Nat. Hazards Rev.* 13 (1), 1–10. [https://doi.org/10.1061/\(ASCE\)NH.1527-6996.0000058](https://doi.org/10.1061/(ASCE)NH.1527-6996.0000058).
- Lillesand, T., Kiefer, R.W., Chipman, J., 2014. *Remote Sensing and Image Interpretation*. John Wiley & Sons, New York.
- Liu, Z., Nadim, F., Garcia-Aristizabal, A., Mignan, A., Fleming, K., Luna, B.Q., 2015. A three-level framework for multi-risk assessment. *Georisk Assess. Manag. Risk Eng. Syst. Geohazards* 9 (2), 59–74. <https://doi.org/10.1080/17499518.2015.1041989>.
- Luettich, R.A., Westerink, J.J., 2004. Formulation and Numerical Implementation of the 2D/3D ADCIRC Finite Element Model Version 44. XX. Retrieved from. https://adcirc.org/adcirc_theory_2004_12_08.pdf.
- Masoomi, H., van de Lindt, J.W., 2016. Tornado fragility and risk assessment of an archetypal masonry school building. *Eng. Struct.* 128, 26–43. <https://doi.org/10.1016/j.engstruct.2016.09.030>.
- Masoomi, H., van de Lindt, J.W., Ameri, M.R., Do, T.Q., Webb, B.M., 2018. Combined wind-wave-surge hurricane-induced damage prediction for buildings. *J. Struct. Eng.* 145 (1), 04018227. [https://doi.org/10.1061/\(ASCE\)ST.1943-541X.0002241](https://doi.org/10.1061/(ASCE)ST.1943-541X.0002241).
- Memari, M., Attary, N., Masoomi, H., Mahmoud, H., van de Lindt, J.W., Pilkington, S.F., Ameri, M.R., 2018. Minimal building fragility portfolio for damage assessment of communities subjected to tornadoes. *J. Struct. Eng.* 144 (7), 04018072. [https://doi.org/10.1061/\(ASCE\)ST.1943-541X.0002047](https://doi.org/10.1061/(ASCE)ST.1943-541X.0002047).
- Merz, B., Kreibich, H., Lall, U., 2013. Multi-variate flood damage assessment: a tree-based data-mining approach. *Nat. Hazards Earth Syst. Sci.* 13, 53–64. <http://doi.org/10.5194/nhess-13-53-2013>.
- Muhari, A., Charvet, I., Tsuyoshi, F., Suppasri, A., Imamura, F., 2015. Assessment of tsunami hazards in ports and their impact on marine vessels derived from tsunami models and the observed damage data. *Nat. Hazards* 78 (2), 1309–1328. <https://doi.org/10.1007/s11069-015-1772-0>.
- NIST, 2011. Disaster and Failure Studies Data Repository. National Institute of Standards and Technology Retrieved from. <https://www.nist.gov/topics/disaster-failure-studies/disaster-failure-studies-data-repository>.
- PEER, 2011. PEER Ground Motion Database. Pacific Earthquake Engineering Research Center. Retrieved from. <http://peer.berkeley.edu/>.
- Pistrika, A.K., Jonkman, S.N., 2010. Damage to residential buildings due to flooding of New Orleans after hurricane Katrina. *Nat. Hazards* 54 (2), 413–434. <https://doi.org/10.1007/s11069-009-9476-y>.
- Pita, G.L., Francis, R., Liu, Z., Mitrani-Reiser, J., Guikema, S., Pinelli, J.-P., 2011. Statistical tools for populating/predicting input data of risk analysis models. In: *Paper Presented at the First International Conference on Vulnerability, Uncertainty, and Risk, Hyattsville, Maryland*.
- Pitilakis, K., Crowley, H., Kaynia, A., 2014. *SYNER-G: Typology Definition and Fragility Functions for Physical Elements at Seismic Risk*, vol. 27 Springer, Netherlands.
- Porter, K., Kennedy, R., Bachman, R., 2007. Creating fragility functions for performance-based earthquake engineering. *Earthq. Spectra* 23 (2), 471–489. <https://doi.org/10.1193/1.2720892>.
- Powell, M.D., Houston, S.H., 1996. Hurricane Andrew's landfall in South Florida. Part II: surface wind fields and potential real-time applications. *Weather Forecast.* 11 (3), 329–349. [https://doi.org/10.1175/1520-0434\(1996\)011<0329:HALISF>2.0.CO;2](https://doi.org/10.1175/1520-0434(1996)011<0329:HALISF>2.0.CO;2).
- Powell, M.D., Houston, S.H., Amat, L.R., Morrisseau-Leroy, N., 1998. The HRD real-time hurricane wind analysis system. *J. Wind Eng. Ind. Aerod.* 77, 53–64. [https://doi.org/10.1016/S0167-6105\(98\)00131-7](https://doi.org/10.1016/S0167-6105(98)00131-7).
- Powell, M.D., Houston, S.H., Reinhold, T.A., 1996. Hurricane Andrew's landfall in south Florida. Part I: standardizing measurements for documentation of surface wind fields. *Weather Forecast.* 11 (3), 304–328. [https://doi.org/10.1175/1520-0434\(1996\)011<0304:HALISF>2.0.CO;2](https://doi.org/10.1175/1520-0434(1996)011<0304:HALISF>2.0.CO;2).
- Reed, D.A., Friedland, C.J., Wang, S., Massarra, C.C., 2016. Multi-hazard system-level logit fragility functions. *Eng. Struct.* 122, 14–23. <https://doi.org/10.1016/j.engstruct.2016.05.006>.
- Reese, S., Bradley, B.A., Bind, J., Smart, G., Power, W., Sturman, J., 2011. Empirical building fragilities from observed damage in the 2009 South Pacific Tsunami. *Earth Sci. Rev.* 107 (1), 156–173. <https://doi.org/10.1016/j.earscirev.2011.01.009>.
- Reese, S., Cousins, W., Power, W., Palmer, N., Tejakusuma, I., Nugrahadhi, S., 2007. Tsunami vulnerability of buildings and people in South Java—field observations after the July 2006 Java tsunami. *Nat. Hazards Earth Syst. Sci.* 7 (5), 573–589. <https://doi.org/10.5194/nhess-7-573-2007>.
- Schmidt, J., Matcham, I., Reese, S., King, A., Bell, R., Henderson, R., Smart, G., Cousins, J., Smith, W., Heron, D., 2011. Quantitative multi-risk analysis for natural hazards: a framework for multi-risk modelling. *Nat. Hazards* 58 (3), 1169–1192. <http://doi.org/10.1007/s11069-011-9721-z>.
- Stone, M., 1974. Cross-validated choice and assessment of statistical predictions. *J. R. Stat. Soc. Ser. B* 111–147. <https://doi.org/10.1111/j.2517-6161.1974.tb00994.x>.
- Suppasri, A., Mas, E., Charvet, I., Gunasekera, R., Imai, K., Fukutani, Y., Abe, Y., Imamura, F., 2013. Building damage characteristics based on surveyed data and fragility curves of the 2011 Great East Japan tsunami. *Nat. Hazards* 66, 319–341. <https://doi.org/10.1007/s11069-012-0487-8>.
- Suppasri, A., Mas, E., Koshimura, S., Imai, K., Harada, K., Imamura, F., 2012. Developing tsunami fragility curves from the surveyed data of the 2011 Great East Japan tsunami in Sendai and Ishinomaki plains. *Coast. Eng. J.* 54 (01) 1250008–1250011–1250008–1250016. <https://doi.org/10.1142/S0578563412500088>.
- Tang, C., Zhu, J., Chang, M., Ding, J., Qi, X., 2012. An empirical–statistical model for predicting debris-flow runoff zones in the Wenchuan earthquake area. *Quat. Int.* 250 (0), 63–73. <https://doi.org/10.1016/j.quaint.2010.11.020>.
- Tomiczek, T., Kennedy, A., Rogers, S., 2014a. Collapse limit state fragilities of wood-framed residences from storm surge and waves during Hurricane Ike. *J. Waterw. Port, Coast. Ocean Eng.* 140 (1), 43–55. [https://doi.org/10.1061/\(ASCE\)WW.1943-5460.0000212](https://doi.org/10.1061/(ASCE)WW.1943-5460.0000212).
- Tomiczek, T., Kennedy, A., Rogers, S., 2014b. Survival analysis of elevated homes on the bolivar peninsula after hurricane Ike. *Bridges* 10, 108–118. <https://doi.org/10.1061/9787084412626.010>.
- Tomiczek, T., Kennedy, A., Zhang, Y., Owensby, M., Hope, M.E., Lin, N., Flory, A., 2017. Hurricane damage classification methodology and fragility functions derived from Hurricane Sandy's effects in coastal New Jersey. *J. Waterw. Port, Coast. Ocean Eng.* 143 (5). [https://doi.org/10.1061/\(ASCE\)WW.1943-5460.0000409](https://doi.org/10.1061/(ASCE)WW.1943-5460.0000409).
- van de Lindt, J.W., Dao, T.N., 2009. Performance-based wind engineering for wood-frame buildings. *J. Struct. Eng.* 135 (2), 169–177. [https://doi.org/10.1061/\(ASCE\)0733-9445\(2009\)135:2\(169\)](https://doi.org/10.1061/(ASCE)0733-9445(2009)135:2(169)).
- van de Lindt, J.W., Taggart, M., 2009. Fragility analysis methodology for performance-based analysis of wood-frame buildings for flood. *Nat. Hazards Rev.* 10 (3), 113–123. [https://doi.org/10.1061/\(ASCE\)1527-6988\(2009\)10:3\(113\)](https://doi.org/10.1061/(ASCE)1527-6988(2009)10:3(113)).
- Vickery, P., Twisdale, L., 1995. Wind-field and filling models for hurricane wind-speed predictions. *J. Struct. Eng.* 121 (11), 1700–1709. [https://doi.org/10.1061/\(ASCE\)0733-9445\(1995\)121:11\(1700\)](https://doi.org/10.1061/(ASCE)0733-9445(1995)121:11(1700)).
- Vickery, P.J., Skerlj, P., Steckley, A., Twisdale, L., 2000. Hurricane wind field model for

- use in hurricane simulations. *J. Struct. Eng.* 126 (10), 1203–1221. [https://doi.org/10.1061/\(ASCE\)0733-9445\(2000\)126:10\(1203\)](https://doi.org/10.1061/(ASCE)0733-9445(2000)126:10(1203)).
- Westerink, J.J., Luettich, R.A., Feyen, J.C., Atkinson, J.H., Dawson, C., Roberts, H.J., Powell, M.D., Dunion, J.P., Kubatko, E.J., Pourtaheri, H., 2008. A basin-to channel-scale unstructured grid hurricane storm surge model applied to southern Louisiana. *Mon. Weather Rev.* 136 (3), 833–864. <https://doi.org/10.1175/2007MWR1946.1>.
- Womble, J., Ghosh, S., Adams, B., Friedland, C., 2006. Advanced Damage Detection for Hurricane Katrina: Integrating Remote Sensing Images and VIEWS Field Reconnaissance. MCEER, Buffalo, NY.
- Zhang, Y., Kennedy, A.B., Tomiczek, T., Yang, W., Liu, W., Westerink, J.J., 2017. Assessment of hydrodynamic competence in extreme marine events through application of Boussinesq–Green–Naghdi models. *Appl. Ocean Res.* 67, 136–147. <https://doi.org/10.1016/j.apor.2017.06.001>.